The Magnetic Correlations and Fluctuations in the Geometrically Frustrated Antiferromagnetic Spinel $CdCr_2O_4$: An Experiment Using the SPINS Triple-Axis Spectrometer

Summer School on Methods and Applications of Neutron Spectroscopy

NIST Center for Neutron Research

Sung Chang, Deepak Singh, and William Ratcliff

June 22-26, 2009

Abstract

We will study the magnetic correlations in the geometrically frustrated antiferromagnetic spinel $CdCr_2O_4$ using inelastic neutron scattering. In so doing, we will gain an an understanding of the principles of Triple-Axis Spectroscopy (TAS) and learn how to analyze the TAS data obtained to extract physical information about the system being studied.

I. INTRODUCTION

One of the most useful properties of neutrons is that they have magnetic moments ($S = \frac{1}{2}$). As a result, neutrons interact with magnetic potentials in materials, which are ascribed to either unpaired electrons or nuclear moments. Contrary to the scattering strength from a nonmagnetic nucleus that is a scalar property, the scattering "strength" from a magnetic potential is in fact a vector property and is proportional to magnetic moment or *spin*. Therefore, orientational periodicity matters as much as positional periodicity for magnetic neutron scattering. If there are no spatial correlations, either orientational or positional, among magnetic moments to be studied, signals from magnetic neutron scattering will be incoherent. This is often the case for nuclear magnetic moments since their potential is strongly localized to each nucleus. On the other hand, electronic magnetic moments are often spatially correlated via long-range Coulomb exchange interactions, resulting in well-defined periodicity.

A. Magnetic structure

Once the positional periodicity of magnetic ions is given from crystal structure, one of the main features of interest in terms of magnetic correlations is the pattern of spin orientations, often called *magnetic structure*, and is one of the most often studied subjects of neutron diffractions. Figure 1 (a) shows disordered magnetic states at two extremes. *Paramagnet* is a state where each spin fluctuates rapidly and randomly without any correlations to its neighbor. Any magnetic material will become paramagnetic at high enough temperatures where the thermal energy is greater than the magnetic energy. The net magnetic moment for each spin will be zero for a time scale larger than the fluctuation. Such a state is similar to gases where the periodicity of atomic positions is lost due to thermal fluctuations. When the temperature is lowered, fluctuations will be suppressed and each magnetic ion will have a non-zero net moment. *Spin glass* is a state where there is no well-defined long-range periodicity even after thermal fluctuations are suppressed. Quite often, however, short-range correlations between nearby magnetic ions should exist, and the absence of long-range order is due mostly to extrinsic reasons. On the other hand, a majority of magnetic materials show long-range periodicity when the temperature is lowered enough. There are

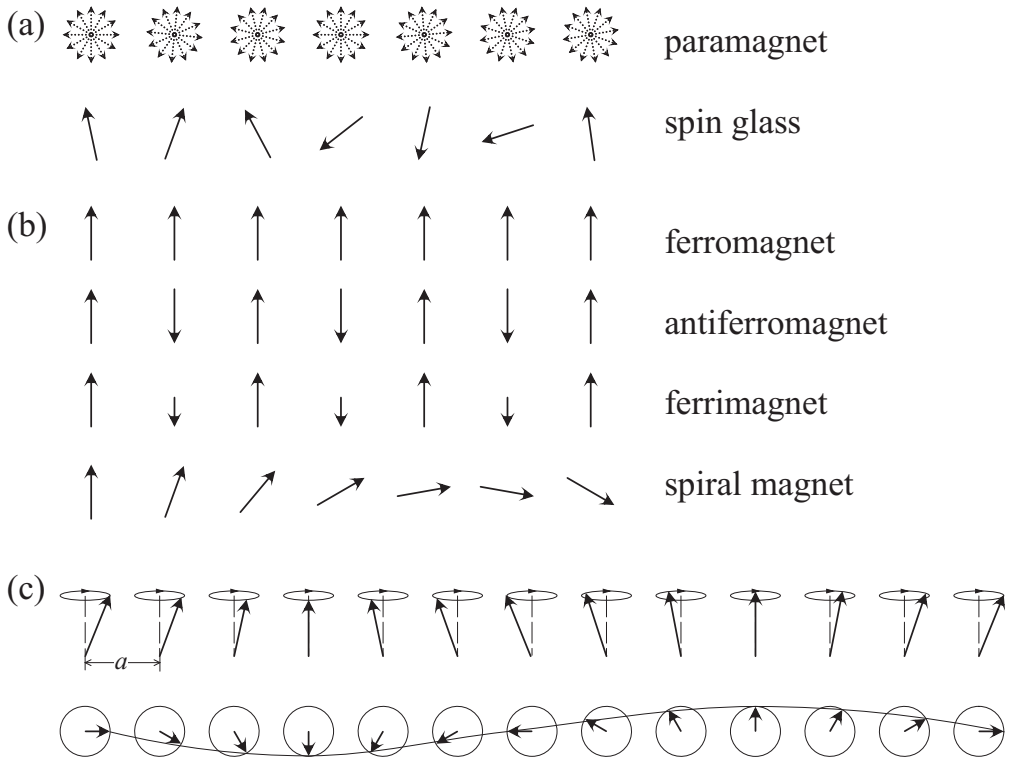

FIG. 1: (a) Schematic illustrations of disordered spin states. (b) Examples of simple magnetic ordering patterns. (c) Classical representation of spin wave excitation in an one-dimensional ferromagnet.

a great diversity of known magnetic structures, yet most of them can be classified into the classes shown in Figure 1 (b). The simplest yet contrasting cases are a ferromagnet and an antiferromagnet, where the nearest neighbor spin correlations are opposite with respect to each other. Additional interactions, for instance, between the second nearest neighbors may induce non-collinear spin structures. The temperature of magnetic transition will depend on the strength of exchange interactions and the size of available spin moments. The strength of the major exchange interactions may be estimated from the temperature dependence of paramagnetic inverse susceptibility ($1/\chi$). (See Figure 2) In antiferromagnets, $1/\chi - T$ curve makes an intercept at $T < 0$, which is referred to as *Curie-Weiss temperature*, Θ_{CW}.

B. Magnetic fluctuations

The magnetic ground state is where the magnetic energy of the system is minimized. Therefore, the ground state magnetic structure must be determined by the magnetic Hamil-

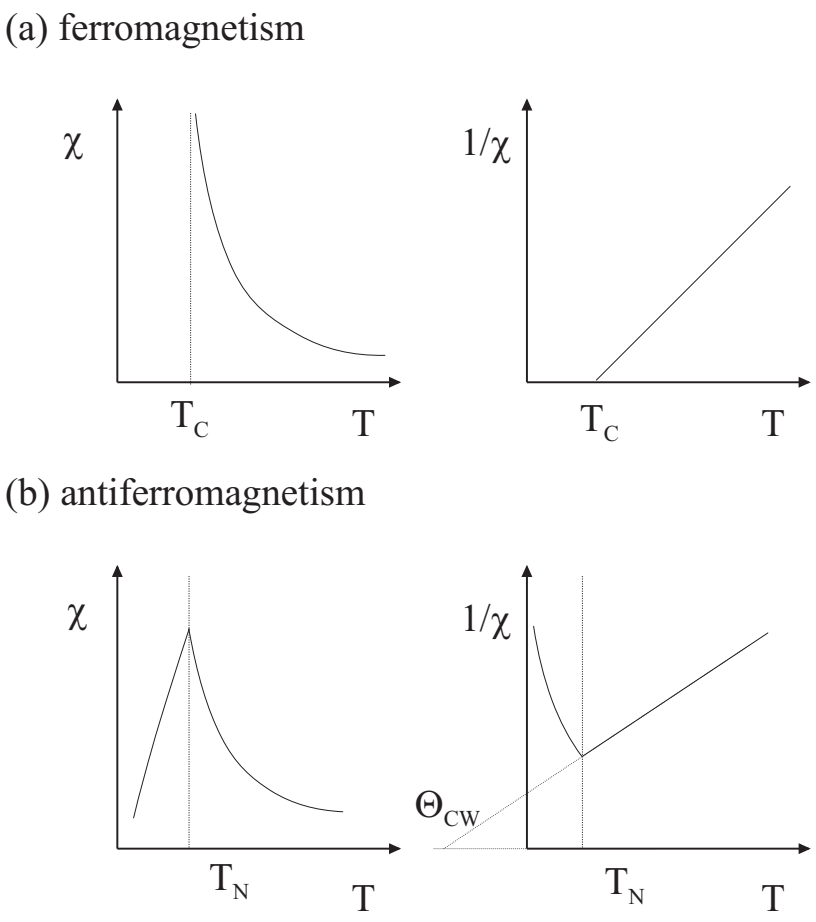

FIG. 2: Typical temperature dependence of magnetic susceptibility $\chi = \partial M/\partial H$ and $1/\chi$ for (a) ferromagnets and (b) antiferromagnets. H and M are applied magnetic field and magnetization of the material, respectively.

tonian that describes the energy of the system. The simplest yet useful form of magnetic Hamiltonian may be written as below:

$$H = -\frac{1}{2}\sum_{i \neq j} J_{ij}\mathbf{S}_i \cdot \mathbf{S}_j, \tag{1}$$

where $\mathbf{S}_i$ and $\mathbf{S}_j$ are magnetic moments at i-th and j-th ions, respectively, and J_{ij} is an isotropic Heisenberg exchange strength constant between them. In the given form, the signs and strengths of J will determine the magnetic structure, that is, $J > 0$ for ferromagnets and $J < 0$ for antiferromagnets.

While the signs of major exchange interactions may be deduced from simply observing magnetic structures, their quantitative strengths can be obtained by measuring spin fluctu-

ations or excitations. It is because such interaction strength will work as a restoring force when spins fluctuate and deviate from their ordered directions. In ordered magnets with isotropic spins, fluctuation of each spin will propagate through the lattice and produce wave-like excitations of finite energy depending on directions of propagation. Although spins and their fluctuations are *quantized* quantities, most of the time their fluctuations can be approximately yet fairly closely understood by mimicking behaviors of classical waves. A *classical* illustration of ferromagnetic *spin wave* propagation is shown in Figure 1 (c). Dynamics of magnetism is not limited to dispersive wave-like excitations, but also includes various localized excitations such as crystal field transitions, singlet-to-triplet excitations, etc. Neutron spectroscopy is, again, one of the most powerful technique to quantitatively investigate the diverse range of magnetic interactions in condensed matter.

The detailed understanding of spin wave excitations is beyond the scope of this experiment. Instead, we will study a different type of magnetic fluctuation arising from magnetic short-range correlations. If magnetic fluctuation of a magnetic ion is hampered from propagating through the lattice for any reason, the fluctuation may be localized and/or decay quickly. For the particular problem to be studied in this experiment, such a localized fluctuation is ascribed to topologically induced spin disorder.

II. BASICS OF NEUTRON SCATTERING

A. Neutron as a probe of matter

It is the ability of the neutron to exchange a *measurable* amount of energy with a liquid or solid sample that makes it useful as a probe of the various dynamical phenomena in condensed matter systems.[1] Typical neutron energies available at a reactor source can range from 100 – 500 meV (hot), to 5 – 100 meV (thermal), to 0.1 – 10 meV (cold), where 1 meV = 10^{-3} eV = 8.06 cm^{-1}. A number of different methods can be used to prepare a monochromatic (or monoenergetic) neutron beam having energies that are comparable in magnitude to, for example, those of the lattice vibrations in a solid (phonons), the spin excitations in a magnetic system (magnons), the torsional, bending, or stretching vibrations of a polymer chain, or the rotational motions in a molecular solid (librons). It is usually quite easy to detect the change in the neutron energy after scattering from a sample since

the energy transferred to or from the sample $\Delta E = E_i - E_f$ generally represents a significant fraction of the initial and final neutron energies E_i and E_f.

The energy ΔE transferred during the interaction between neutron and sample can be used to create an excitation (such as a phonon or magnon) of the system, in which case the neutron loses an amount of energy ΔE equal to the energy of the excitation. Conversely, the same excitation can give up its energy to the neutron, in which case the excitation is said to be annihilated. In either case, the physics of the excitation as revealed by the absolute change in the neutron energy is the same. The energy transfer ΔE is often expressed as a frequency of vibration through the relation

$$\Delta E = \hbar\omega, \tag{2}$$

where $2\pi\hbar = h = 6.626 \times 10^{-34}$ Joules-seconds is Planck's constant, and ω is the frequency of vibration of the excitation. Since frequency and time are inversely related, the neutron energy transfer $\hbar\omega$ reflects the *time scale* of the dynamics.

Question: Estimate the value of $(\Delta E/E_i)$ required to observe an optic phonon with an energy of 10 meV using x-ray, light, and neutron scattering techniques assuming the values of E_i = 7,000 eV, 2 eV, and 30 meV (0.030 eV), respectively. Which technique is best suited for this measurement?

In addition to having energies that are well adapted to the study of a large variety of dynamical phenomena, neutrons also possess the ability to provide, simultaneously, unique information about the *geometry* of these dynamics through the exchange of momentum with the sample. This is done by measuring in what directions (i. e., through what angles) the neutrons scatter. The momentum of a neutron varies inversely with the neutron wavelength λ, and hence an accurate measure of the momentum transferred between sample and neutron during the scattering process will in turn provide information about the spatial scale of the dynamics being probed. Such an accurate measure is relatively easy to obtain as long as the neutron wavelength is comparable to the length scale of the motions of interest.

Question: The relationship between wavelength and energy for the neutron is given by:

$$E = \frac{h^2}{2m\lambda^2} = 81.81(\text{meV} \cdot \text{Å}^2)/\lambda^2, \tag{3}$$

where $m = 1.675 \times 10^{-24}$ grams is the mass of the neutron. Using this equation, estimate the wavelengths corresponding to hot, thermal, and cold neutrons available at a reactor source. How do these wavelengths compare with the length scales associated with the dynamics or motions you are specifically interested in?

In the following sections we will discuss the partial differential scattering cross section, which is the actual physical quantity that is measured by neutron spectroscopy. We then outline the basic operating principles behind a triple-axis spectrometer (TAS), the concept for which Bertram Brockhouse earned the 1994 Nobel prize in physics shared jointly with Clifford Shull.

B. The Partial Differential Scattering Cross Section $\frac{\mathrm{d}^2\sigma}{\mathrm{d}\Omega \mathrm{d}E_f}$

Most neutron spectroscopic techniques can be reduced to a measurement of what is called the *partial differential scattering cross section*, or $\mathrm{d}^2\sigma/\mathrm{d}\Omega\mathrm{d}E_f$, as a function of the neutron energy transfer $\hbar\omega$ and the neutron momentum transfer $\mathbf{Q}$.[1] The quantity $\mathbf{Q}$ is known as the scattering vector, and has units of inverse length. In the scattering process between the neutron and the sample, the total momentum and energy of the system are conserved, i.e.

$$\mathbf{Q} = \mathbf{k_i} - \mathbf{k_f}, \tag{4}$$

$$\hbar\omega = E_i - E_f = \Delta E. \tag{5}$$

Hence the energy or momentum lost (or gained) by the neutron when it scatters from a sample is gained (or lost) by the sample. In the previous equation, the quantities $\mathbf{k_i}$ and $\mathbf{k_f}$ refer to the initial and final neutron wavevector, respectively, and point in the direction of the incident and final (scattered) neutron beam. The relationship between $\mathbf{k_i}$, $\mathbf{k_f}$, and $\mathbf{Q}$ can be represented by the *scattering triangle* shown in Fig. 3. The magnitude of the neutron wavevector k is $2\pi/\lambda$, and is related to the neutron energy via

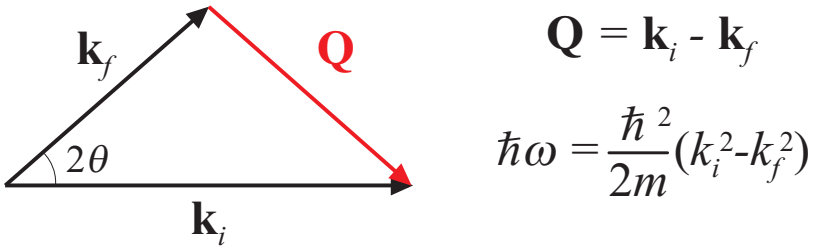

FIG. 3: Scattering triangle. The neutron is scattered through the angle 2θ and the scattering vector, $\mathbf{Q}$, is given by the vector relationship $\mathbf{Q} = \mathbf{k}_i - \mathbf{k}_f$.

$$E = \frac{(\hbar k)^2}{2m} = 2.072k^2[\text{meV} \cdot \text{Å}^2], \tag{6}$$

From this last equation, one can obtain the second equation in Fig. 3 which relates the energy transfer to the magnitude of the initial and final wavevectors. The angle between $\mathbf{k}_i$ and $\mathbf{k}_f$ is commonly denoted by 2θ, and represents the total angle through which a neutron is scattered by the sample. Note that the convention followed in this summer school is such that the energy transfer $\hbar\omega$ is positive when $E_i > E_f$, i. e. when the neutron loses energy to the sample during the scattering process. This convention of defining when $\hbar\omega$ is positive varies among neutron scattering facilities.

The partial differential scattering cross section is defined as the total number of neutrons scattered per second by the sample into a unit of solid angle $\mathrm{d}\Omega$ in a given direction, having final energies E that lie between E_f and $E_f + \mathrm{d}E_f$. It is normalized by the neutron flux incident on the sample Φ_0 (measured in neutrons/sec/cm^2) so that it has units of area/(solid angle)/energy. If one integrates the partial differential scattering cross section over the entire solid angle ($= 4\pi$ steradians), and all final energies ($0 \leq E_f \leq \infty$), one obtains the total number of neutrons scattered out of the beam per second by the sample. (This assumes that the absorption of neutrons by the sample, which can often occur, is negligible.) This is known as the total scattering cross section σ, which has units of area. Thus σ represents the scattering strength of the sample, and can be viewed as an unnormalized probability that an incident neutron will be scattered. If one compares the value of σ for hydrogen with that of aluminum, it will be clear that different elements can have enormously different scattering strengths.

Question: The scattering cross section for x-rays is a strong and monotonically increasing function of atomic number Z. This is because x-rays scatter from the electrons of an atom, which increases with increasing Z. Neutrons, by contrast, scatter from the atomic nucleus via short-range nuclear forces. If you plot σ for neutrons versus Z, do you see any trend? In what ways might this be advantageous? (Values for σ can be obtained from the NCNR Summer School web page under "Course Materials," or at http://www.ncnr.nist.gov/resources/n-lengths/.)

It is instructive to consider the relative sizes of σ and $\mathrm{d}^2\sigma/\mathrm{d}\Omega\mathrm{d}E_f$. Clearly σ, which represents the total number of neutrons scattered per second by the sample, is many orders of magnitude larger than $\mathrm{d}^2\sigma/\mathrm{d}\Omega\mathrm{d}E_f$, which is an analyzed quantity both in energy and direction. On the other hand, the partial differential scattering cross section provides a correspondingly greater amount of information because it contains all of the details of the individual and collective motions of the atoms, molecules, and/or any atomic magnetic moments that comprise the sample. The *differential cross section* $\mathrm{d}\sigma/\mathrm{d}\Omega$, which is what is measured in a diffraction experiment, lies between σ and $\mathrm{d}^2\sigma/\mathrm{d}\Omega\mathrm{d}E_f$ in size. As the elastic component dominates in $\mathrm{d}\sigma/\mathrm{d}\Omega$, it gives the time-averaged (equilibrium) positions of all of the nuclei in the sample, and is used to determine the crystal structure.

The partial differential scattering cross section can be cast into a useful mathematical form via the formalism outlined at the end of the neutron scattering primer written by Roger Pynn[2] (which the summer student is presumed to have read). With a small deviation from the notation used by Pynn we can write the partial differential cross section for a system composed of a single atomic element as

$$\frac{\mathrm{d}^2\sigma}{d\Omega\mathrm{d}E_f} = \frac{1}{4\pi}\left(\frac{k_f}{k_i}\right)\left[\sigma_{coh}S_{coh}(\mathbf{Q},\omega) + \sigma_{inc}S_{inc}(\mathbf{Q},\omega)\right], \tag{7}$$

where $S(\mathbf{Q},\omega)$ is exactly same quantity as $I(\mathbf{Q},\epsilon)$ used by Pynn to express Van Hove's *scattering law*. The subscripts *coh* and *inc* refer to the coherent and incoherent parts of the scattering, and pertain to the collective or individual motions of the atoms, respectively, as described on page 9 of Pynn's primer. Whenever spatial correlation of scatterers is of interest, however, the coherent term only needs to be considered.

The scattering function $S_{coh}(\mathbf{Q},\omega)$ contains a double sum over pairs of nuclei as shown

in Eq. 3 on page 28 of Pynn's primer.[2] Each term in this sum represents the *correlation* between the position of one nucleus at a time $t = 0$ with that of another nucleus at an arbitrary time t later. These correlations are important for systems in which the nuclei are strongly coupled via some type of interaction, and less so when this coupling is weak. In either case $S_{coh}(\mathbf{Q}, \omega)$ provides a measure of the strength of this coupling, and hence the resulting *collective* motions. It is therefore extremely useful, for example, in mapping out the dispersion relations of lattice vibrations, that is how the energy $\hbar\omega$ of the lattice vibrations changes at different $\mathbf{Q}$ positions, in solids. For the remainder of this discussion, we will drop the subscript *coh* with the understanding that we are referring to the coherent part of the scattering function.

The scattering function $S(\mathbf{Q}, \omega)$ can be simply related to the imaginary part of the dynamical susceptibility according to

$$S(\mathbf{Q}, \omega) = \frac{\hbar}{\pi} \left(\frac{1}{e^{\hbar\omega/k_B T} - 1} + 1 \right) \chi''(\mathbf{Q}, \omega), \tag{8}$$

where $k_B = 1.381 \times 10^{-23}$ Joules/K is Boltzmann's constant (note: $\hbar/k_B = 11.60$ K/meV is a handy conversion factor). This is a very important equation since it shows that $S(\mathbf{Q}, \omega)$, which is readily obtained from the experimentally measured partial differential scattering cross section via Eq. (7), is also related to a quantity that is easily calculated by theorists, $\chi''(\mathbf{Q}, \omega)$. The dynamical susceptibility is a measure of how the system responds when it is "wiggled". $\chi''(\mathbf{Q}, \omega)$ refers to the imaginary part of this quantity, which is related to how energy is dissipated by the system. Therefore a measurement of the partial differential scattering cross section via neutron spectroscopy allows for a direct test of theoretical models. By recording the scattered neutron intensity as a function of energy transfer $\hbar\omega$ and momentum transfer $\mathbf{Q}$, and removing the instrumental effects, one obtains $S(\mathbf{Q}, \omega)$, which contains all of the dynamical information about the system.

With the exception of the neutron spin-echo (NSE) technique, all other neutron spectroscopic methods measure $\mathrm{d}^2\sigma/\mathrm{d}\Omega\mathrm{d}E_f$ using a neutron detector to count the number of neutrons scattered per unit time from a sample as a function of the energy transfer $\Delta E = \hbar\omega$ and the momentum transfer $\mathbf{Q}$. To do this requires that one knows the energy and wavevector of the neutron before $(E_i, \mathbf{k_i})$ and after $(E_f, \mathbf{k_f})$ it scatters from the sample. There are many ways of doing this, and most will be illustrated by the different experiments in this summer school. As will be seen, each method has its own particular advantages and limi-

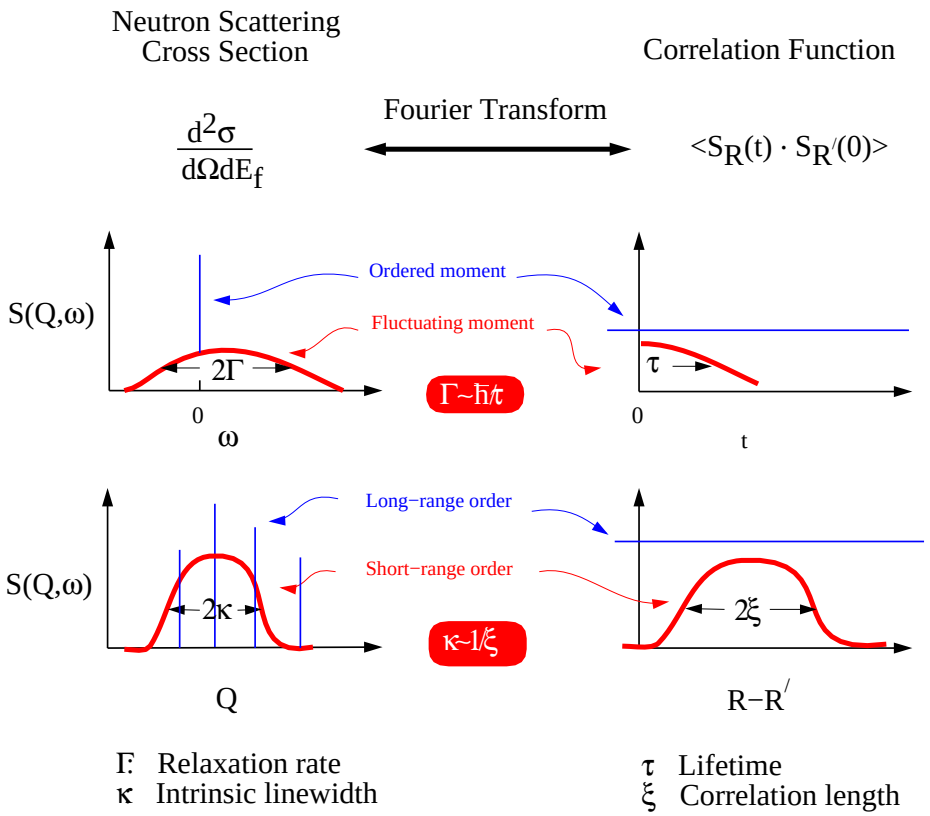

FIG. 4: The relationship between the neutron scattering cross section and the spin-spin correlation function. The relaxation rate Γ is HWHM in energy of $S(Q,\omega)$, and is inversely proportional to the lifetime of the excitation τ. The line-width κ is the HWHM in momentum transfer of $S(Q,\omega)$, and is inversely proportional to the correlation length ξ.

tations, depending on the range of energy transfers (time scales) and momentum transfers (length scales) one wishes to study.

C. Understanding The Spin-Spin Correlation Function $\langle S_R(t) \cdot S_{R'}(0) \rangle$

The intensity of neutrons scattered from the magnetic moments in a solid is proportional to the spin-spin correlation function:[1]

$$\begin{aligned} \frac{\mathrm{d}^2\sigma}{\mathrm{d}\Omega \mathrm{d}E_f} &= r_0^2 \frac{k_f}{k_i} |\frac{g}{2} F(Q)|^2 \sum_{\alpha\beta} (\delta_{\alpha\beta} - \hat{Q}_\alpha \hat{Q}_\beta) \\ &\times \frac{1}{2\pi\hbar} \int dt \; e^{i\omega t} \frac{1}{N} \sum_{\mathbf{R}\mathbf{R}'} \left\langle S^\alpha_{\mathbf{R}}(t) S^\beta_{\mathbf{R}'}(0) \right\rangle e^{-i\mathbf{Q}\cdot(\mathbf{R}-\mathbf{R}')} \end{aligned} \tag{9}$$

where $r_0 = -0.54 \cdot 10^{-12}$ cm, g is the gyromagnetic ratio, $F(Q)$ is the magnetic form-factor and N is the number of unit cells in the solid. Basically the partial differential scattering cross section $\mathrm{d}^2\sigma/\mathrm{d}\Omega\mathrm{d}E_f$ is the Fourier transform in space and time of the spin-spin correlation function $\langle S_R(t) \cdot S_{R'}(0)\rangle$. Thus, neutron elastic scattering probes static ordered moments, whereas neutron inelastic scattering probes fluctuating (dynamic) moments.

While this equation appears formidable, Fig. 4 can help shed substantial light on the relationship between the measured magnetic neutron scattering cross section and the time-dependent spin-spin correlation function. The spatial dependence of the spin correlations can be determined from the Q-dependence of $S(\mathbf{Q},\omega)$. For example, if $S(\mathbf{Q},\omega)$ is Q-resolution limited, then this would indicate that the spatial correlations are of long-range. However, if $S(\mathbf{Q},\omega)$ is broader than the instrumental Q-resolution, then the correlations are short-ranged. A similar argument can be made for linewidths, which is the peak widths observed in energy scans. If $S(\mathbf{Q},\omega)$ is $\hbar\omega$-resolution limited, then this would indicate that the temporal correlations are of long-range. However, if $S(\mathbf{Q},\omega)$ is broader than the instrumental $\hbar\omega$-resolution, then the excitations are only short-lived in time.

III. TRIPLE-AXIS SPECTROSCOPY

A. Introduction to The Triple-Axis Spectrometer

The triple-axis spectrometer (TAS) is an extremely versatile instrument that is primarily intended for the study of the collective motions of the atoms and their magnetic moments in single crystal samples. The first TAS system was used to obtain the first experimental demonstration of phonon and magnon dispersion curves (in aluminum and magnetite) in the mid 1950's.[3] The instrument derives its name from the fact that the neutrons interact with three crystals on their way from reactor to detector, each crystal being able to rotate independently about a vertical axis passing through its center. This is shown schematically in Fig. 5. The first crystal is called the monochromator, as it selects a single monochromatic component from the white neutron beam emanating from the reactor or neutron guide. The second crystal is the sample itself (although it may be either a single crystal or a powder). The third crystal is called the analyzer, as it is used to analyze the energy spectrum of the neutron beam that scatters from the sample. The last primary element of the instrument

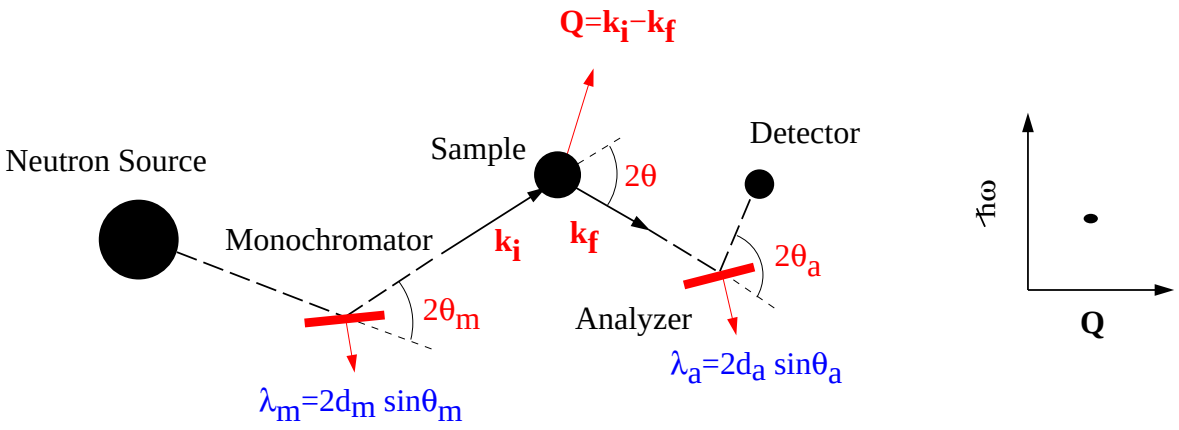

FIG. 5: Schematic scattering configuration for a conventional triple-axis spectrometer. It measures a scattering event at a single value of $(\mathbf{Q}, \hbar\omega)$ at a time.

is, of course, the neutron detector.

In a triple-axis spectrometer, the initial and final neutron energies are determined by exploiting the process of Bragg diffraction from the monochromator and analyzer single crystals. This is done by rotating the crystals about their respective vertical axes such that a specific set of atomic Bragg planes, having a well-defined interplanar spacing d, makes an angle θ, known as the Bragg angle, with respect to the initial (or scattered) beam direction. When this is done, only neutrons with wavelengths that satisfy the Bragg condition (see pages 9-11 of Pynn's primer)

$$n\lambda = 2d\sin\theta, \tag{10}$$

where n is an integer greater than zero, will Bragg scatter from each crystal and proceed successfully to the next element of the spectrometer.

Question: Because the variable n in Bragg's law can be any integer greater than zero, more than one monochromatic component can be present in the neutron beam diffracted by either monochromator or analyzer. List the possible wavelengths of these other components. How might their presence affect the experimental data?

To remove the extra and unwanted monochromatic components from a Bragg diffracted beam, while preserving the neutron flux at the desired fundamental (n=1) wavelength λ,

it is common practice to place a filter composed of some solid material in the path of the beam. The choice of material depends on the primary wavelength λ. For thermal neutrons, a special form of graphite (pure carbon) known as highly-oriented pyrolytic graphite (HOPG or just PG) is often used. Graphite has a layered structure in which the crystalline [001] or c-axis is normal to the layers. HOPG behaves like a crystal of graphite in which the various graphite layers have all been randomly spun about the c-axis. Therefore HOPG can be viewed as a single-crystal along [001], and a powder along the two orthogonal directions. It exhibits very good transmission at certain neutron energies including 13.7, 14.7, 30.5, and 41 meV. Neutrons of other energies are preferentially (though not completely) scattered out of the beam, thereby minimizing the chance they will enter the detector and contribute to the background.

For cold neutrons, such as those used on the SPINS spectrometer, a polycrystalline block of beryllium (Be) or beryllium oxide (BeO) is used as a wavelength filter. The requirement for this filter to work is that there be enough tiny crystallites to span all angular orientations, *i.e.* all values of the Bragg angle θ, so that all unwanted neutrons are Bragg scattered out of the neutron beam.

Question: (1) Consider a white (polychromatic) beam incident on a polycrystalline Be filter. What happens to those neutrons with wavelengths $\lambda > 2d_{max}$, where $d_{max} = 1.98$ Å is the largest interplanar d spacing available in beryllium? What happens to those neutrons with $\lambda \leq 2d_{max}$? Make a simple sketch of transmission versus energy for this filter.
(2) What are the criteria for ideal materials for designing neutron low-pass filters?

As can be seen from Fig. 5, when the incident neutron beam from the reactor strikes the monochromator, it is scattered through an angle $2\theta_m$ from its initial direction. This is commonly referred to as the monochromator *scattering angle*. In order for the resulting monochromatic beam to hit the sample, it is necessary to rotate the subsequent elements (sample, analyzer, and detector) of the spectrometer about the monochromator axis through an angle of $2\theta_m$. The same situation applies for the sample, and the analyzer, i. e. associated with each crystal is a Bragg angle θ, and a scattering angle 2θ. Hence each axis of the triple-axis spectrometer is actually composed of two motors, one to control the crystal Bragg

angle θ, and the other to rotate the subsequent (downstream) elements of the instrument by the appropriate scattering angle 2θ. While there are many different motors involved in the operation of a triple-axis spectrometer, such as those that control mechanical slits that limit the horizontal and vertical extent of the neutron beam, the primary instrument motors are those that control the values of θ and 2θ for the monochromator, sample, and analyzer. (NOTE: The convention of naming θ and 2θ comes from the fact that $2\theta = 2 \times \theta$ for elastic Bragg scattering. Even though this relation no longer holds for inelastic scattering, they are still called the same way.)

The material most commonly used as monochromator and analyzer in a TAS system is also HOPG. Its utility lies in its very high reflectivity for neutrons over a wide range of energy, along with its negligible incoherent scattering and adsorption cross sections, and its low atomic number so that scattering by gamma rays is small. The (002) Bragg planes of HOPG have an interplanar d spacing of 3.354 Å. Other materials that also find use in triple-axis spectroscopy are silicon, germanium, and copper.

Question: Calculate the monochromator Bragg and scattering angles required to obtain a neutron beam having initial energies $E_i = 14.7$ meV, and 100 meV using the (002) reflection of HOPG. The (220) reflection of copper has a d spacing of 1.278 Å. Would this be a better choice of monochromator in either case?

During the interaction with the sample, neutrons can lose or gain energy, and thus can emerge with an energy $E_f \neq E_i$. The resulting energy transfer can be computed according to

$$\hbar\omega = E_i - E_f = \frac{h^2}{8m}\left(\frac{1}{d_m^2 \sin^2\theta_m} - \frac{1}{d_a^2 \sin^2\theta_a}\right), \tag{11}$$

where d_m and d_a are the d-spacings of the monochromating and analyzing crystals, respectively. If the analyzer is set to select the same energy as that of the incident beam ($E_i = E_f$), then $\hbar\omega = 0$, and the scattering is said to be *elastic*. If not, one detects *inelastic* scattering events.

Measuring the momentum transfer $\mathbf{Q}$ between neutron and sample is achieved by orienting the incident and final neutron wavevectors with respect to each other to obtain the desired vector difference ($\mathbf{k_i} - \mathbf{k_f}$). Unlike the case of the monochromator and analyzer crystals,

the Bragg and scattering angles for the sample needn't be related by a simple factor of 2. Indeed, when measuring inelastic scattering they usually are not. Hence the notation 2θ (which is quite common) can be misleading for the novice scatterer. With this warning in mind, we can calculate the magnitude of the momentum transfer from the scattering triangle diagram in Figure 3 as below.

$$Q = \sqrt{k_i^2 + k_f^2 - 2k_i k_f \cos 2\theta}. \tag{12}$$

Note that the momentum transfer does not depend on the sample Bragg angle θ, but only on the sample scattering angle. The purpose of the Bragg angle is to allow the crystalline axes of the sample (if it happens to be a single crystal) to be aligned in specific ways with respect to the scattering vector $\mathbf{Q}$. This allows one to probe the geometry of the dynamics in question along different symmetry directions. The utility of the sample Bragg angle becomes moot, however, in the case of a powder sample (composed of many tiny and randomly-oriented single crystals).

Question: What is the maximum momentum transfer one can obtain in the case of elastic scattering, i.e. $|\mathbf{k}_i| = |\mathbf{k}_f|$? What is the minimum? Why might these two configurations be problematic from an experimental point of view?

By stepping the analyzer Bragg angle θ_a, or the monochromator Bragg angle θ_m, by computer in small angular increments, one can effectively scan the energy transfer $\hbar\omega$. Generally this is done while keeping the momentum transfer $\mathbf{Q}$ constant, and is known as a constant-$\mathbf{Q}$ scan. The complement to the constant-$\mathbf{Q}$ scan is the constant-E scan in which the energy transfer is held constant while one varies the momentum transfer. These two scans are fundamental to the triple-axis method, and are used commonly to map out the dispersion relations for both phonons and magnons in condensed matter systems.

In the case of a constant-$\mathbf{Q}$ scan, one has the choice of fixing either the incident or final energy, through fixing the Bragg angles of either the monochromator or the analyzer. As a rule, it is best not to vary both as one needs to place a wavelength filter in the path of either the incident beam (before the sample) or the scattered beam (after the sample) in order to remove the higher order harmonic content of the Bragg diffracted neutron beam

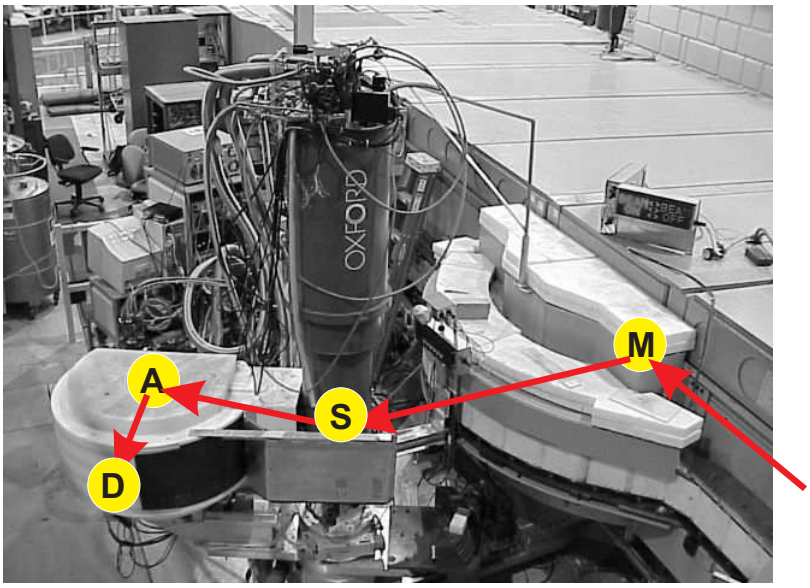

FIG. 6: Overview of the SPINS spectrometer. The arrows show the path of the neutron beam during a scattering experiment. M, S, A, and D stand for monochromator, sample, analyzer, and detector.

(remember the effect of the integer n in Bragg's law). If the analyzer angle θ_a is fixed and one varies θ_m, the result is an E_f-fixed configuration. Doing the opposite results in an E_i-fixed configuration. Both methods yield data that contain the same physics. Deciding which to choose depends largely on the specific problem being studied.

B. The NCNR Spin Polarized Inelastic Neutron Scattering (SPINS) Spectrometer

SPINS is a cold-neutron triple-axis spectrometer. Fig. 6 show an overview of the SPINS spectrometer and the schematics of the neutron path. Its incident energy range can be changed between 2.4 and 14 meV. The monochromator of SPINS consists of 5 blades of PG crystals can vertically focus incoming neutron flux to a sample with a size smaller than the height of the beam. On the other hand, the analyzer consists of 11 blades also of PG crystals that are standing vertically in a row and can individually be rotated. Taking advantage of this multi-crystal analyzer, SPINS is designed to operate in various configurations including (1) conventional triple-axis mode, (2) horizontally focusing analyzer mode, and (3) multiplexing mode. Since many components of the SPINS instrument can be changed as necessary, other modes not described here are also possible. For instance, polarized-neutron

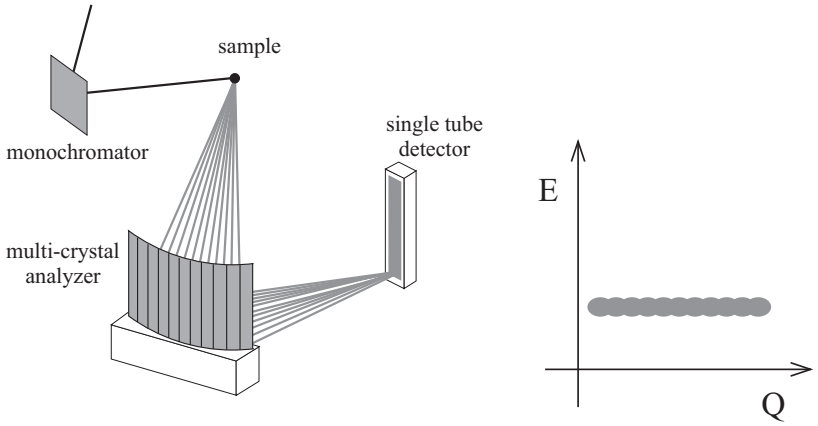

FIG. 7: Schematic scattering configuration of a horizontally focusing analyzer mode utilizing a multi-blade analyzer for a triple-axis spectrometer. It collects intensity from a broad range of momentum transfer simultaneously while maintaining a good energy resolution.

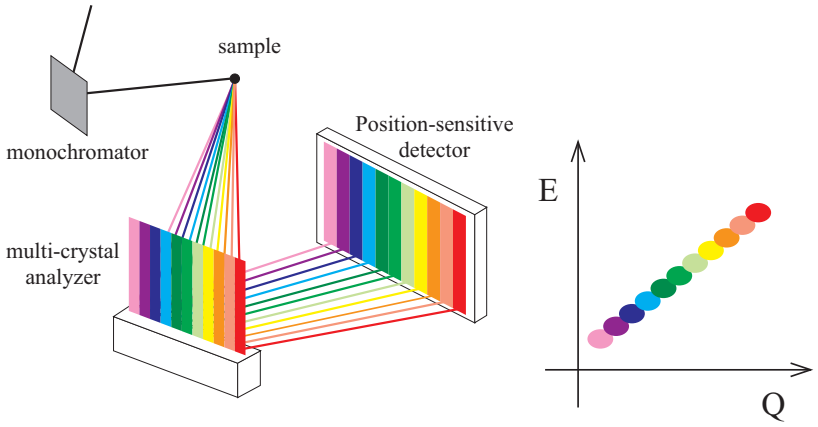

FIG. 8: Schematic scattering configuration of a multiplexing detection system utilizing a Position-Sensitive-Det spectrometer. It simultaneously measures scattering events at different values of $(\mathbf{Q}, \hbar\omega)$.

scattering mode is also optionally available.

(1) Conventional triple-axis mode has been discussed previously, and shown in Fig. 5. At SPINS, it can be achieved by using just a few analyzer blades in the middle, typically three, which are aligned flatly with respect to each other. A single tube detector is used with necessary collimators through the beam path.

(2) Horizontally focusing analyzer mode is schematically shown in Figure 7. The basic idea of this mode is to focus scattered neutrons over a wide solid angle into a single tube detector. It has an effect of relaxing momentum resolution while maintaining energy reso-

TABLE I: Comparison chart of neutron scattering spectrometers at NCNR in terms of the needs for this particular experiment.

Issues	SPINS	BT7/9	DCS	HFBS	NSE	FANS
$\lvert\Theta_{CW}\rvert \approx 88$ K corresponds to $J \approx 1$ meV	◯	×	◯	×	×	×
$S(\mathbf{Q},\omega)$ at well-defined $\mathbf{Q}(hkl)$ space	◯	◯	△	×	×	×
diffraction can also be done with good resolution	◯	△	×	×	×	×

lution. As a result, detected neutron intensity will increase roughly proportionally to the number of the focusing blades. It is very efficient in data collection rate when the features to be measured are broad in momentum space. Ideally the blades need to be positioned on an arc of a circle encompassing the positions of the sample and the detector, so that Bragg angles for all the blades are equal. In practice, one can achieve an approximate focusing condition by placing the row of the blades tangential to the relevant arc, and maintain a constant incident angle of neutrons for each blade. The momentum resolution can be adjusted by appropriately selecting the number of focusing blades.

(3) In multiplexing modes, a wide area of the position sensitive detector (PSD) is used together with the multi-crystal analyzer. In the most typical setup, schematically shown in Figure 8, the 11 analyzer blades are aligned in such a way to scatter neutrons into equally-spaced columns on the PSD. If the blade arrangement is nearly flat as in Figure 8, each blade will have a different Bragg angle and subsequently a different energy. Therefore, signal from each blade will correspond to both different momentum and different energy transfers. The positional sensitivity of the PSD can efficiently discriminate this information. This mode is very efficient in data collection when momentum dependence of excitation is two-dimensional or less. Typically a calibration run should be performed for a given setup using an incoherent scatterer, and used as a reference for energy and intensity calibrations. Various creative combinations of the analyzer-PSD setups are possible depending on the necessity of the experiment.

At NCNR there are several neutron scattering spectrometers with diverse experimental capabilities that are available to internal and external users. Whenever neutron scattering experiment is planned, it is very important to consider various aspects of experimental needs and select the best suited instrument. Table I summarizes the most important reasons why

SPINS, the cold neutron triple-axis spectrometer, is the best instrument for this particular study in comparison with other instruments. An additional advantage of using SPINS is that various experiments requiring different experimental configurations, such as elastic versus inelastic, high versus low Q resolution, and high versus low energy resolution, can be performed in series on the same instrument.

IV. SPIN FLUCTUATIONS IN GEOMETRICALLY FRUSTRATED ANTIFERROMAGNETIC SPINEL $CDCR_2O_4$

A. Geometrically frustrated magnets

In certain magnetic materials, magnetic order would not appear even when the system is cooled down much below the temperature comparable to the major exchange strength. In this experiment we are particularly interested in the case where crystal structure is responsible for the suppression of magnetic order, which is often called *geometrical frustration*. As the simplest example, consider a case where antiferromagnetic spins are placed on an equilateral triangle as in Figure 9 (a), and assume only two spin orientations are allowed, either up or down. After placing the first two spins antiparallel to each other, the third spin cannot simultaneously satisfy antiferromagnetic correlations with the two other spins. It is often said that the third spin is *frustrated*. In fact, it is not just the third spin but the three-spin system that is frustrated, and there are more than one lowest energy state possible for the given system. Such topologically induced multiply degenerate ground states that prevent the system from ordering is a characteristic of geometrically frustrated magnets. One of the most well known examples is realized in the case of the corner-shared network of tetrahedra found for spinel (AB_2O_4) B sites. (See Figure 9 (b)) Due to the intricate network of infinite number of triangles, antiferromagnetic order cannot be stabilized even for isotropic Heisenberg spins where any orientation of spins is allowed.

Most geometrically frustrated magnets will eventually order when the temperature is lowered enough. It is often realized by structural distortions that reduce crystal symmetry. Frustration factor, $f = |\Theta_{CW}|/T_N$, is usually larger than 10 for most frustrated magnets. In the temperature range between T_N and $|\Theta_{CW}|$, the system is in a supercooled state where a strong tendency for establishing long-range magnetic order is held back by reasons other

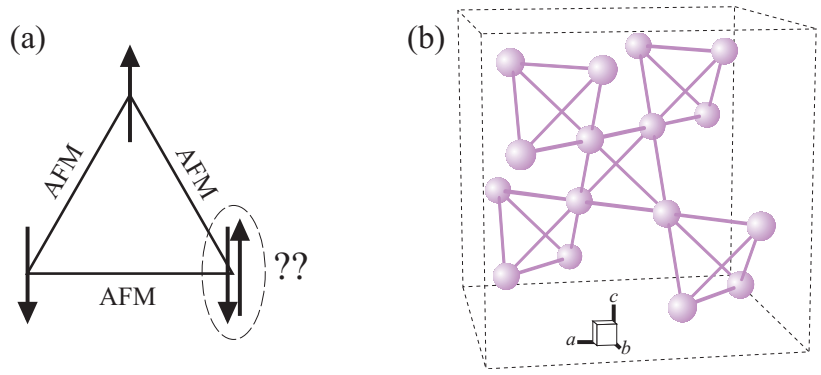

FIG. 9: (a) Three spins on a triangle cannot simultaneously satisfy antiferromagnetic correlations with all of their neighbors. (b) Spinel B sites form a corner-shared network of tetrahedra, which consists of many edge-shared triangles. It is often called a pyrochlore lattice.

than thermal fluctuations. This suggests that each ion will possess a finite magnetic moment and interact strongly with neighboring ions, contrary to usual paramagnets. Therefore, via neutron scattering one may expect to observe short-range magnetic correlations, both in space and in time, and fluctuations between multiple degenerate ground states.

Question: Consider the case of a triangular lattice with isotropic Heisenberg spins. If nearest neighbor exchange is antiferromagnetic, is geometrical frustration expected or not?

B. Spin-Peierls-like phase transition in chromate spinels

Spinels with Cr^{3+} ions on B sites are good examples to study geometrical frustration.[4–7] It is because Cr^{3+} ion has three electrons in its $3d$ orbital. Under the 6-coordinated oxygen environment as in spinels, these three electrons will equally populate d_{xy}, d_{yz}, and d_{zx} wave functions, corroborating an isotropic cubic environment. Therefore, electronic orbitals will have no effect in distorting cubic symmetry. In contrast, spinels with V^{3+} ($3d^2$) ions on B sites are well known to have orbitally driven structural phase transitions due to their freedom to selectively populate two out of three available wave functions.[8] Such absence of orbital degrees of freedom in chromate spinels is intriguing in two aspects. One is that its frustration factor is maximized because orbital effects will not help, and the other is that

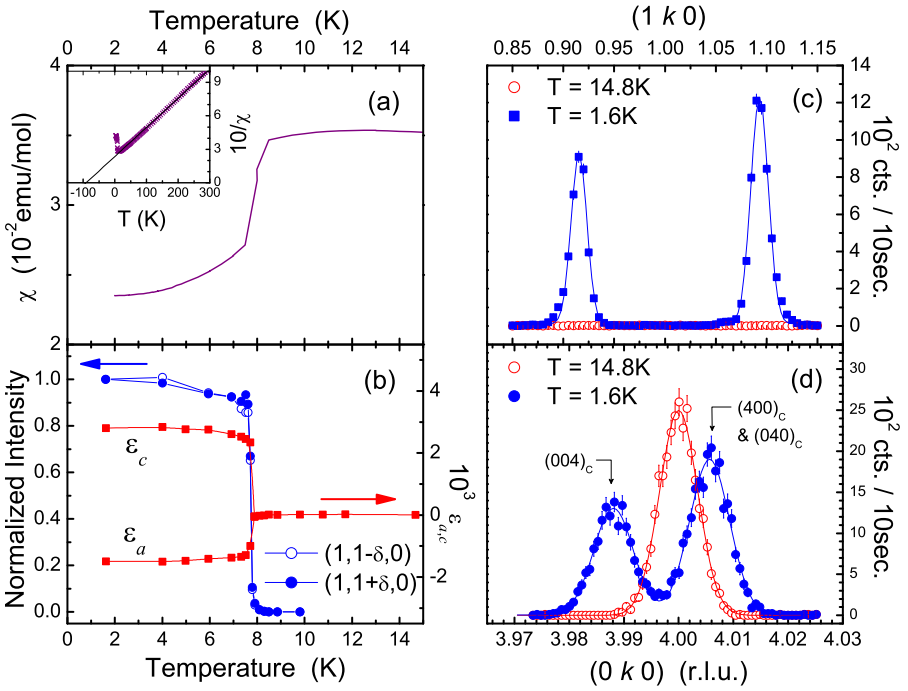

FIG. 10: (a) Bulk susceptibility, χ, as a function of T. The inset shows a linear fit to $1/\chi$. (b) T-dependence of the normalized neutron scattering intensity at the magnetic peaks and that of the lattice strains. The data were obtained from fitting the data in (c) and (d) to gaussians. (c), (d) Elastic neutron scattering data (c) through incommensurate magnetic (1,δ,0) reflections and (d) through a nuclear (400) Bragg reflection below and above T_N. (From Ref. 7)

an observed structural transition will most likely be ascribed to the reduction of magnetic energy alone.

$ZnCr_2O_4$ has a Curie-Weiss temperature $|\Theta_{CW}| \approx 390$ K, while its magnetic transition occurs at temperatures as low as $T_N = 12.5$ K.[4] The estimated frustration factor is as large as $f \approx 31$, demonstrating a large degree of geometrical frustration. The lifting of frustration is achieved via a cubic-to-tetragonal lattice distortion ($c < a = b$) that simultaneously occurs with the magnetic transition. Such contraction along the c axis conveniently explains the reduction of magnetic energy by satisfying four antiferromagnetic correlations out of six.[6] Experimentally, however, magnetic order shows up with multiple ordering wave vectors and the true ground state spin structure is yet to be revealed. In this experiment, we investigate a closely related compound $CdCr_2O_4$ where only the non-magnetic A site ion

is replaced. Since ionic distances are increased due to the larger Cd ion, its magnetic interactions are weaker than in $ZnCr_2O_4$, that is $|\Theta_{CW}| = 88$ K and $T_N = 7.8$ K. (See Figure 10 (a)) Quite surprisingly, however, its cubic-to-tetragonal distortion ($c > a = b$) occurs along the direction opposite to the one observed in $ZnCr_2O_4$, and the magnetic order is incommensurate with a single wave vector $\mathbf{k} = (1,\delta,0)$, $\delta \approx 0.09$. (See Figure 10 (b)-(d)) Such diversity in magnetic transitions from geometrically frustrated chromate spinels demonstrate the complexity of the antiferromagnetic interactions in pyrochlore systems.

V. EXPERIMENT AND ANALYSIS

A. Experimental Planning and Setup

The purpose of this experiment is to understand the nature of magnetic fluctuations of geometrically frustrated antiferromagnetic spinels. From the combination of elastic and inelastic neutron scattering measurements, we will be able to identify the spatial and temporal correlations of both spin-frustrated and spin-ordered phases. We chose $CdCr_2O_4$ as a model system to study. While its frustration factor is smaller than that of $ZnCr_2O_4$, we prefer $CdCr_2O_4$ because it has a well-defined magnetic order with a single ordering wave vector. The notorious problem of any sample containing cadmium is that naturally occurring cadmium has a prohibitively high neutron absorption cross section. Fortunately, such high absorption is ascribed only to ^{113}Cd, which is 12.22 % in natural abundance. Therefore, we will use single crystal samples enriched with ^{114}Cd for neutron scattering.

While the energy of the analyzer may be arbitrarily chosen for triple-axis spectrometers, the typical energy of the analyzer at SPINS is either 5.0 meV or 3.7 meV. This is mostly because these numbers are just below the cut-off energies of low-pass Be and BeO filters, respectively. One may access wider momentum space with reasonable intensity with $E_f = 5.0$ meV, while better energy resolution is obtained with $E_f = 3.7$ meV. The low-pass filters are inserted between the sample and the analyzer, and will prevent scattered high-energy neutrons from entering analyzer-detector assembly and leaving spurious experimental artifacts. For elastic scattering an additional low-pass filter is usually inserted between the monochromator and the sample.

A single crystal sample of $^{114}CdCr_2O_4$ has been oriented in the $hk0$ scattering geometry,

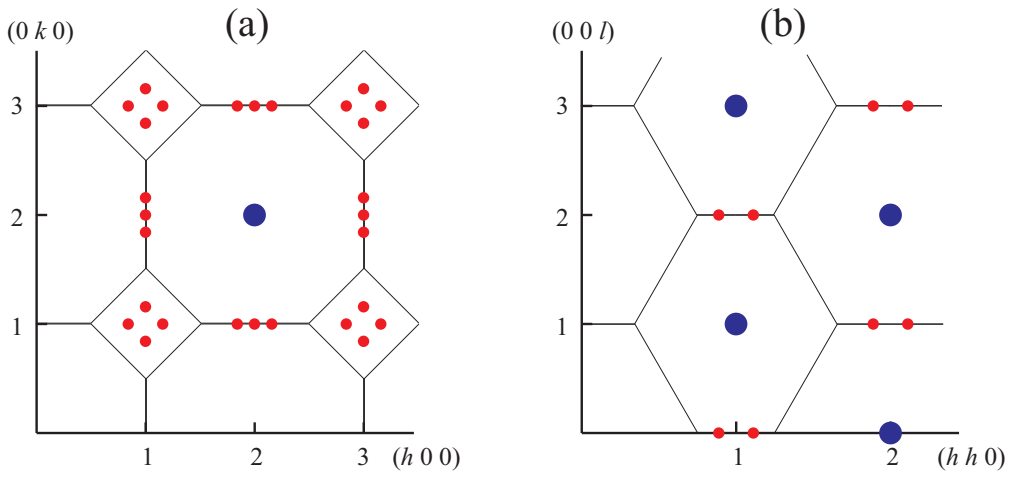

FIG. 11: Reciprocal space planes of $CdCr_2O_4$ in the (a) $hk0$ and (b) hhl scattering geometries. Large blue and small red dots mark positions of nuclear and magnetic Bragg peaks, respectively. The solid lines are Brillouin zone boundaries.

where the cubic a and b axes are located in the horizontal scattering plane. (See Figure 11 (a)) An alternative orientation is the hhl scattering geometry, where one of the two axes are rotated out of the horizontal plane by 45^o while the other remains. (See Figure 11 (b)) In the case of inelastic scattering, three pieces of crystals were co-aligned and mounted together to enhance scattering intensity. The samples are then sealed in a He-filled aluminum can and cooled down by a liquid-He filled cryostat. The instrument will be operated in fixed-E_f mode with $E_f = 5.0$ meV. The instrumental configuration for inelastic measurements following the neutron path downstream is: neutron guide–monochromator–80' collimator–sample–Be filter–radial collimator–11 blade horizontally focusing analyzer–detector (G–80'–Be–RC–11HFA–D in short). The energy resolution for the above configuration is about 0.3 meV.

B. Data and analysis

Figure 12 shows the energy dependence of magnetic inelastic neutron scattering intensity measured at $\mathbf{Q} = (1\ 1\ 0)$ above and below $T_N = 7.8$ K. The neutron scattering spectrum at $T = 15$ K, which is above T_N and in the spin disordered phase, is featureless and very broad in energy. This means that the magnetic fluctuation at this temperature is quasi-elastic in nature and short-lived in time. We can roughly estimate the relaxation rate Γ, which is

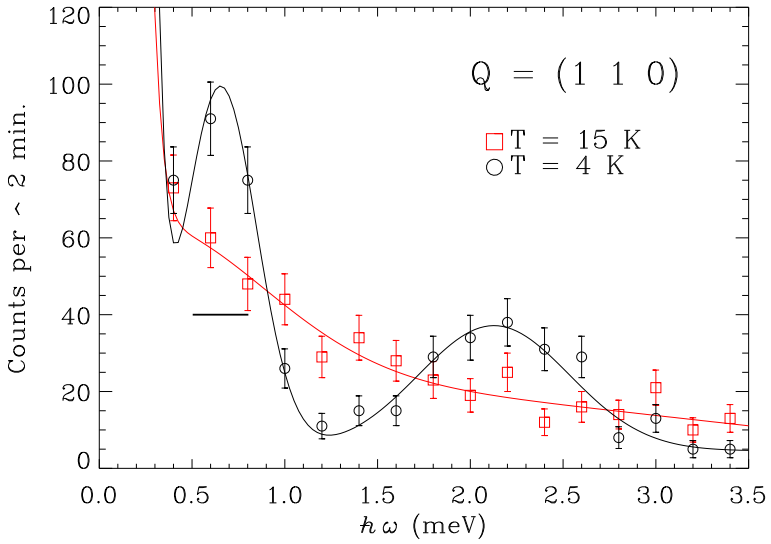

FIG. 12: Inelastic neutron scattering intensity at $\mathbf{Q} = (1\ 1\ 0)$ of $CdCr_2O_4$ as a function of energy transfer. The red square and black circle point are measured above and below T_N, respectively. The lines are guides to the eye. The thick and short horizontal bar is the experimental resolution width.

the Half-Width-at-Half-Maximum (HWHM) of $S(\omega)$: $\Gamma \approx 2$ meV. One may estimate the lifetime of the dynamic correlations at this temperature to be $\hbar/\Gamma \sim 0.3 \cdot 10^{-12}$ s. On the other hand, the spectrum at $T = 4$ K, which is below T_N and in the spin ordered phase, shows well defined peaks at $\hbar\omega = 0.65$ meV and 2.1 meV. Particularly, the width of the peak at 0.65 meV is comparable to the instrumental resolution. It means that these are normal modes of spin wave vibrations arising from cooperative thermal fluctuations of ordered spins.

The spatial dependence of the dynamic spin-spin correlation function can be obtained by observing momentum dependence of the inelastic neutron scattering intensity. Spin wave dispersions will always show minima at magnetic Bragg peak positions, since momentum transfer around those positions correspond to long-wavelength in-phase fluctuations of ordered spins. The understanding of spin wave dispersions from antiferromagnetic spinels, however, is a very complicated problem. Instead, we will try to understand the dynamic spin-spin correlation function in the spin frustrated phase. Figure 13 (a) shows the contour of inelastic neutron scattering intensity measured on the $hk0$ plane of $CdCr_2O_4$ at $\hbar\omega = 0.6$ meV and $T = 15$ K. The apparent strong momentum dependence of the inelastic intensity is evidence that there is a good deal of spatial correlation between the spins in the

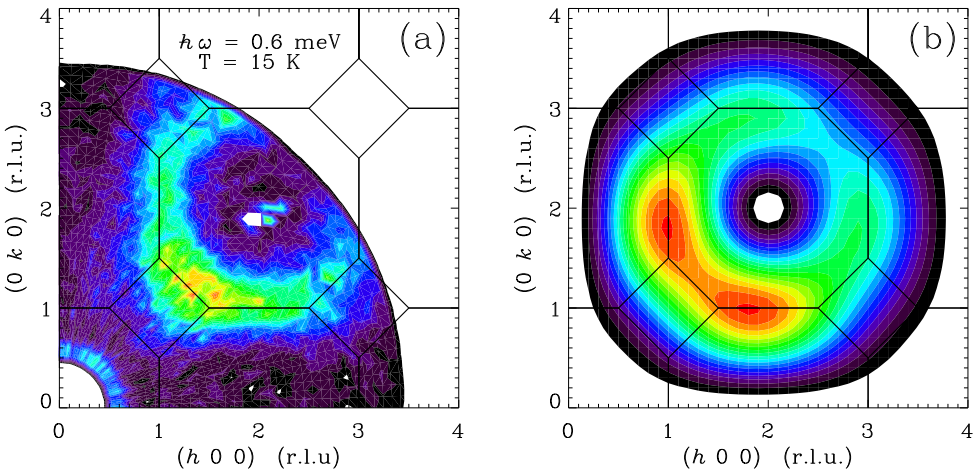

FIG. 13: (a) Momentum dependence of inelastic neutron scattering intensity, $\hbar\omega = 0.6$ meV, measured in the spin frustrated phase of $CdCr_2O_4$. (b) Magnetic neutron cross section calculated from the equation of antiferromagnetic hexagon ring that is described in the text. The solid lines are Brillouin zone boundaries.

supposedly disordered phase and strongly suggests that the fluctuations in the geometrically frustrated phase is far from being random. While the magnetic ordering wave vector for the spin ordered phase is (0 δ 1) with $\delta << 1$, the fluctuation pattern does not form around either (0 0 1) or (1 1 0). Instead, it forms a large ring around (2 2 0), and thus is distinctly different from spin wave excitations in the ordered phase.

To understand the spatial correlations of the observed fluctuations, we calculate the dynamical part of the magnetic structure factor and compare with the experimental data. Since the fluctuation is supposed to be quasi-elastic in nature, one may use the static correlation function ($t \to \infty$) derived from Equation (9), which is essentially equal to the square of the magnetic structure factor as below.

$$\frac{d\sigma}{d\Omega} \propto |F(Q)|^2 \sum_{\alpha\beta}(\delta_{\alpha\beta} - \hat{Q}_\alpha \hat{Q}_\beta) \sum_{\mathbf{R}\mathbf{R}'} S^\alpha_{\mathbf{R}} S^\beta_{\mathbf{R}'} e^{-i\mathbf{Q}\cdot(\mathbf{R}-\mathbf{R}')} \tag{13}$$

$$\propto |F(Q)\sum_{\mathbf{R}}(\mathbf{S}_{\mathbf{R}})_{\perp}e^{-i\mathbf{Q}\cdot\mathbf{R}}|^2$$

Above, $\mathbf{S}_{\perp} = \hat{\mathbf{Q}} \times (\mathbf{S} \times \hat{\mathbf{Q}})$, which means that only the spin components perpendicular to the momentum transfer vector contribute to the magnetic neutron scattering cross section. Assuming there is no spin anisotropy for the fluctuation in the frustrated cubic phase, the above equation can be further simplified by simply replacing $\mathbf{S}_{\perp}$ with $\mathbf{S}$. Since the correlation of the fluctuation is supposed to be short-ranged, it is straightforward to enter the coordinates of the magnetic ions and spin orientations into the above equation and calculate the momentum dependence of the quasielastic neutron scattering cross sections. There may be several possible candidate models for short-range antiferromagnetic fluctuations, such antiferromagnetic pairs, antiferromagnetic chains, tetrahedra, etc.. Students will be given a code to perform these model calculations, but also are welcome to write their own code and/or try out the solutions analytically. Figure 13 (b) is a calculation using an antiferromagnetic hexagonal loop model, which best describes the experimental data. The considered model consists of six antiferromagnetic spins forming a hexagon. The analytical formula for the neutron cross section is given as follows.

$$\begin{aligned} |F(\mathbf{Q})|^2 \propto & \{\sin\frac{\pi}{2}h \cdot (\cos\frac{\pi}{2}k - \cos\frac{\pi}{2}l)\}^2 \\ + & \{\sin\frac{\pi}{2}k \cdot (\cos\frac{\pi}{2}l - \cos\frac{\pi}{2}h)\}^2 \\ + & \{\sin\frac{\pi}{2}l \cdot (\cos\frac{\pi}{2}h - \cos\frac{\pi}{2}k)\}^2 \end{aligned} \tag{14}$$

During the Summer School experiments, students will take another set of data in the *hhl* scattering geometry, compare with the model calculation, and see whether or not the antiferromagnetic hexagon model correctly describes the nature of the fluctuation.

In order to understand the temperature dependence of this short-range spin correlation, we have performed inelastic neutron scattering measurements along the [h h 0] direction at various temperatures. Figure 14 (a) shows that as the temperature is increased the intensity gradually decreases while the peak width does not change noticeably. From the plot of integrated intensity shown in Figure 14 (b), we see that this short-range spin correlation shows up at a temperature near $|\Theta_{CW}| = 88$ K. Therefore, we conclude that the nearest neighbor antiferromagnetic exchange interactions is responsible for this short-range spin fluctuation.

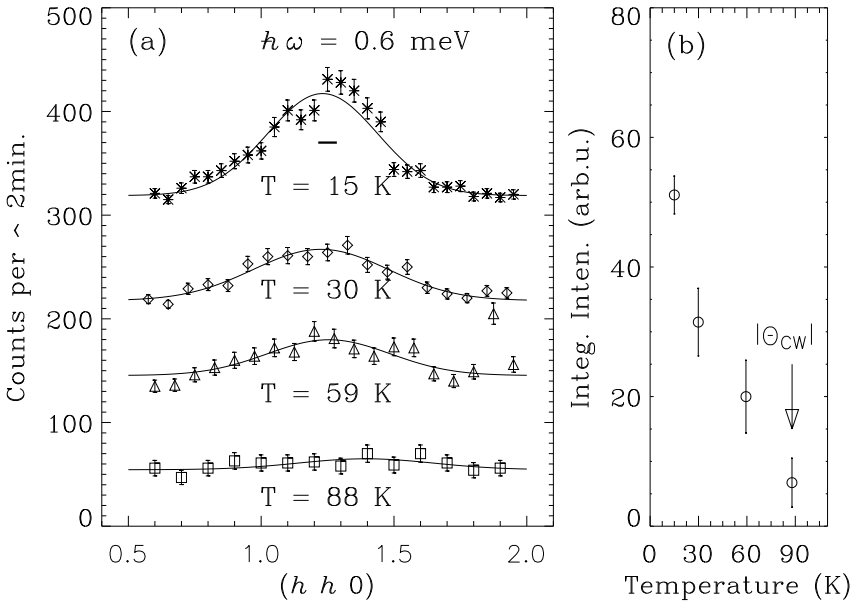

FIG. 14: (a) Momentum-dependence of the inelastic neutron scattering intensity measured at various temperatures below Θ_{CW} and at $\hbar\omega = 0.6$ meV. The solid lines are fits to Gaussians. The short horizontal bar below the data at T = 15 K is the experimental resolution. (b) The integrated intensity from the fittings in (a) as a function of temperature.

VI. SUMMARY

Triple-axis spectroscopy is one of the most widely used neutron scattering techniques for studying lattice and magnetic dynamics in condensed matter. Its strength is in its capability to measure $S(\mathbf{Q}, \omega)$ at desired momentum and energy transfers with great flexibility. In this experiment, we have studied the geometrically frustrated antiferromagnetic spinel $CdCr_2O_4$. Its frustrated magnetism is characterized by a large difference between two characteristic temperatures, $|\Theta_{CW}| = 88$ K and $T_N = 7.8$ K. Below T_N, where a long-range antiferromagnetic order is established via a cubic-to-tetragonal lattice distortion ($c > a = b$), spin wave excitations can be observed at finite energy transfers by inelastic neutron scattering. A resolution-limited line shape is observed for such excitations, suggesting that these spin waves are long-lived in time. Between T_N and $|\Theta_{CW}|$, on the other hand, the magnetic fluctuation showed a very broad spectrum both in energy and momentum. It is consistent with the presence of short-range and short-lived magnetic clusters in the spin disordered phase. By comparing model calculations of magnetic neutron scattering cross section and experimental quasielastic scattering intensity, we find that the spin fluctuation in the geo-

metrically frustrated cubic spinel can be understood as short-range cooperative fluctuations of hexagonal antiferromagnetic spin loops.

---

[1] S.W. Lovesy, *Theory of Neutron Scattering from Condensed Matter*, Oxford, (1984).

[2] R. Pynn, *Neutron Scattering - A Primer*, Los Alamos Science Summer (1990).

[3] B.N. Brockhouse, Rev. Mod. Phys. **67**, 735751 (1995).

[4] S.-H. Lee, C. Broholm, T. H. Kim, W. Ratcliff II, and S-W. Cheong, Phys. Rev. Lett. **84** 3718 (2000).

[5] S.-H. Lee, C. Broholm, W. Ratcliff, G. Gasparovic, Q. Huang, T. H. Kim and S.-W. Cheong, Nature **418** 856 (2002).

[6] O. Tchernyshyov, R. Moessner, and S. L. Sondhi, Phys. Rev. Lett. **88** 067203 (2002).

[7] J.-H. Chung, M. Matsuda, S.-H. Lee, K. Kakurai, H. Ueda, T. J. Sato, H. Takagi, K.-P. Hong, and S. Park, Phys. Rev. Lett., **95** 247204 (2005)

[8] S.-H. Lee, D. Louca, H. Ueda, S. Park, T. J. Sato, M. Isobe, Y. Ueda, S. Rosenkranz, P. Zschack, J. Iñiguez, Y. Qiu, and R. Osborn *et al.*, Phys. Rev. Lett., **93**, (2004) 156407.